IMPROVED METHODOLOGY FOR THE CHARACTERIZATION OF COMPLEX VUGGY CARBONATE

A. Bersani, B.B. Bam, F. Radaelli and E. Rossi
ENI E&P

ABSTRACT

This paper shows the workflow used to find a relationship between lithofacies – as defined independently in the sedimentological study – and petrophysical behaviour: an essential tool to distribute the petrophysical properties in the vuggy carbonate reservoir. Conventional and special core analyses (including gas permeabilities along six different horizontal directions) have been performed on a set of whole core samples taken from cores recovered in the Carboniferous section of a field in Kazakhstan. The data obtained have been integrated with imaging techniques (X Ray-CT and Magnetic Resonance imaging), pore throat size distribution form mercury intrusion, pore network characterization and sedimentological/petrographical study to obtain a univocal description of the poro-permeable system.
This work highlights the anisotropy of these carbonates according to size, percentage and spatial distribution of vugs and fractures, resulting in significantly different orders of magnitude of permeability: from less than 0.01 to hundreds of millidarcies.
Tomographic techniques resulted determinant to discriminate isolated from touching vug porosity and individuate the main elements responsible for permeability anisotropy.
The comparison of different scales of observation suggested significant differences in the dynamic behaviour between the lithofacies as defined in the sedimentological study. At reservoir scale, different fluid flow pathways are expected for "in situ bioherm" facies compared to "reworked bioherm-related facies", even when they have similar poro/perm values at the core scale. This innovative "integrated multi scale approach" developed by ENI is proved to be more effective and reliable for vuggy carbonate characterization.

INTRODUCTION

Vuggy carbonates are extremely heterogeneous; their petrophysical behaviour is a non linear result of different types of porosity, both primary - inter particle and intra particle – and secondary, represented by molds, vugs, touching vugs and microfracturing.
The difficulties due to the extreme heterogeneity of the porous/permeable system exceeding the core dimension are well documented (Jennings, 2008; Knackstedt et al., 2006; Vizika et al., 2007), but even if there are many excellent studies that tackle the question and suggest solutions, they still remain a big issue.
This study does not intend to reinvent the wheel, but provide a further contribution to the promotion of an integrated approach, which exploits the capabilities of conventional and "unconventional" tools, working at different scales, providing a reliable description of the petrophysical properties consistent with the 3D geological model of the reservoir.

In addition to conventional core analysis, geological description, fracture analysis and imaging techniques were introduced. In fact, the utility of X-ray CT and NMR imaging techniques in characterizing complex porous systems has been demonstrated (Radaelli et al., 1998; Bona et al., 2002; Withjack et al., 2003); in particular, they have been applied in characterizing complex vuggy carbonates (Bona et al. 2003; Bye et al., 2008; Hidajat et al., 2004; Vik et al., 2007).

PROCEDURES

Our data set is composed of 15 preserved whole cores (length 30-40 cm) recovered in the Carboniferous section of a Pre-Caspian Basin well. Taking into account a typical depositional model of an isolated carbonate platform, the samples were described as representative of two main environments: bank margin and lower slope. They were classified according three main depositional facies groups (see Tab. 1): in-situ biohermal deposits (here indicated as MBDST) and reworked biohermal deposits, distinguished between fine grained (GRST/PKST) and coarse grained (RDST). As already said, these samples are extremely heterogeneous and their petrophysical behaviour is a complex result of different types of porosity, both primary (inter/intraparticle) and secondary, represented by molds, vugs, touching vugs and microfractures.

Sample selection

The samples were selected with different density and size of vugs on the basis of preliminary X-ray CT images acquired on whole cores.

For each preserved sample, a set of 3 companion samples was cut:

- 15 full size cores (4 inches in diameter, 4-4.5 inches in length) for porosity, dual porosity, permeability, X-ray CT and NMR tomography,
- 15 plugs (1.5 inches in diameter, 2 inches in length) for oil-brine capillary pressure determination
- 15 plugs (1 inch in diameter, 1 inch in length) for pore throat size distribution by mercury intrusion.

Sample preparation, permeability and porosity

The samples were cleaned by hot solvent refluxing and dried in an oven at 110°C. Porosity was determined by the re-saturation method and a correction was applied for surface vugs. Multiple directional gas permeability measurements were acquired on each sample: one vertical and six transversal arranged 30° apart. A Hassler-type core holder was used with a lateral screen subtending a 15° angle. The geometrical factor was experimentally determined using homogeneous samples with known permeability. All the measurements were carried out at ambient conditions, the effect of confining stress has not yet been investigated. With this methodology, it is possible to evaluate the permeability anisotropy within the cored interval. The comparison among different directional permeabilities measured on the same sample remains valid despite possible experimental error.

These measurements were compared with the directions of recognized fracture events, to verify, in a tangible way, possible sample directionality (the permeability being a vector quantity) and evaluate the weight of different factors contributing to fluid flow.

X ray-Computer Tomography
The X-ray images were acquired with a fourth-generation Picker PQS medical CT scanner, using a single energy level of 130 KVp and 100 mA. The spatial resolution was about 0.5 mm with a slice thickness of 1 mm. To obtain reliable results, the scanner was carefully calibrated to optimise with "beam hardening correction". It is important to choose the uniform reference materials with a mineralogical composition as similar as possible to the investigated lithology. Calibration scans must be acquired with the same scanner setup (slice thickness, energy, acquisition time, etc.) as the core samples.
The experimental procedure initially provides the acquisition of a preliminary overview pilot image (radiograph scan) of the core taken through the full thickness. 3D acquisitions on whole core samples were then carried out.
On the 15 full size samples three-dimensional acquisitions were acquired. They consisted of multiple 2D contiguous images (cross-section slices, transverse to the axis of the core), with a slice thickness of 1 mm, taken every 0.5 mm and partially overlapped to improve the quality of data (signal to noise ratio). All these two-dimensional images (about 200 slices for each sample) have been post-processed using a commercial software called Avizo. For details, refer to:
www.tgs.com/products/docs/Avizo_Geoscience_TechOverview.pdf
A 3D volume of the data set was reconstructed and visualized for each sample. From the 3D volume, six different transversal planes (with a thickness of 10 mm) were extracted, corresponding to the six transversal directions with interval of 30° where absolute gas permeability was measured.
The unrolled X-ray CT image of the external surface of the sample was also provided, to be compared with fracture traces visually observed.

Capillary pressure
Primary drainage (oil-displacing-water) capillary pressure curves were acquired on plug samples of diameter 1.5 inches at different 8 capillary pressure increments from 0.2 to 12 bar. Measurements were performed at ambient conditions using a Beckman high speed Ultracentrifuge. The fluids used were brine (salinity 150 g/l) and Soltrol 130 oil from CPchem; the brine-oil interfacial tension was 46 dyne/cm.
To eliminate any error in the calculation of inlet-face saturations due to boundary effects at the outlet end, a Teflon cushion was used to maintain the proper outlet conditions. As discussed in the literature (Hirasaki et al. 1992), a teflon endpiece is as effective as a footbath.
Sufficient time was allowed at each rotational speed to establish saturation equilibrium within the samples. Equilibrium at each speed was determined by monitoring displaced brine volumes during centrifugation using a strobe unit mounted in the rotational chamber.
To derive capillary pressure/saturation data from the measured production profile, the "Forbes 2nd method with radial correction" was used for solving the centrifuge equation. This method was proven to be the most accurate, as a SCA survey demonstrated (Forbes 1997).
 A J-function was then obtained from the measured data as:

$$J(Sw) = Pc(Sw)(\sqrt{k/\varphi} / \sigma \cos \vartheta)$$

(1)

Pore throat distribution
Pore throat distribution was carried out by mercury intrusion tests (MICP) using an automatic system (Micromeritics' AutoPore IV) operating at mercury injection pressures

up to 60,000 psi. To calculate the pore throat size distribution, the Washburn equation was used:

$$D=(1/P)4\gamma\cos\vartheta \qquad (2)$$

Corrections were finally made for "surface conformance effects". All samples are surrounded by a zone of surface roughness and exposed pore surface voids (e.g. external vugs) that are generally large and not related to the sample's interconnected pore system; such surface voids, however, can be filled by mercury at the beginning of the test (first pressure steps). Since they can affect the calculation of both incremental and cumulative saturations, it is necessary to correct the raw data for these "surface conformance effects".

The injection pressure was plotted vs. mercury saturation for each of the analysed samples. Inflections of the curves were recognised and pore throat size distribution functions corrected by subtracting the contribution of low pressure-apparent mercury intrusion.

Moreover, results of pore network analysis previously performed were used to define in great detail the poro-permeable characteristics of the matrix *sensu stricto* at the smallest available scale of observations, comparable with mercury intrusion data.

Magnetic Resonance Imaging (MRI)

The MRI images in the carbonate samples were acquired using a Bruker Biospec 24/40 image spectrometer with the main magnetic field of 2.4 Tesla. The acquisitions were performed on brine-saturated full size samples. A multi-slice multi-echo MSME (15-20 slices, 5mm thickness, matrix 128x128) based on CPMG sequences was used. The MRI signal (Mo) is proportional to the number of nuclei present in the analyzed region and calculated as:

$$M(t) = Mo \exp(-t/T2) \qquad (3)$$

where T2 is transverse relaxation time and t is echo time.

The porosity calculation by means of a reference sample is done by applying the following formula:

$$\varphi_{core}=\varphi_{ref}*(V_{ref}M_{core}/V_{core}/M_{ref}) \qquad (4)$$

The discrimination of different types of porosity (matrix, fractures and vugs) can be done starting from MRI sample images by using proprietary software developed in-house. The classification algorithm uses a combination of statistical and probabilistic approaches that permits the different structures to be recognized by means of their geometrical characteristics (Mattiello et al., 1997). Structures such as vugs/fossils, fractures, and different heterogeneity types can be recognized.

Fracture analysis at core scale

To verify the microfracturing impact on permeability, we calculate a fracture density value, defined through the P21 index, which is the cumulative trace length / unit area, expressed in m/m^2. The measurement is obtained by drawing the fracture traces visible on the external core surfaces and calculating the ratio between sum of these and total lateral area of the sample.

DATA ANALYSIS

The basic petrophysical data are shown in Tab. 1 subdivided by depositional facies. The capillary pressure tests showed a wide range of remaining water values at Pc of 12 bar (from 5 to 76 %), with a fair trend with permeability for all depositional facies (RDST, GRST/PKST and MBDST) as displayed in Fig. 1. The Leverett J function calculated

shows quite a good correlation for the depositional facies RDST and GRST/PKST (Fig. 2) with a regression coefficient R^2 greater than 0.8 (the regression was carried out on samples of both RDST and GRST/PKST facies). The Leverett J data of MBDST facies are quite dispersed as shown in Fig. 3.
The pore throat distributions study was carried out on small plugs (1 inch in diameter, 1 inch long), therefore only rock matrix was characterized. The pore throat distributions from MICP showed for all the samples a broad distribution starting from 0.01 to 50-100 µm without any trend with the depositional facies.

The tomographic images (both MRI and X-Ray) data were used qualitatively only, forsaking the initial purpose of distinguishing and quantifying the percentage of dissolution enlarged porosity. We observed that the presence of large irregular vugs on the external core surface (see Fig. 4) caused significant loss of water during long MRI data acquisitions. But only the comparison between MRI and X-Ray images highlighted that the water loss also affected internal pores in an unforeseeable way. The internal vugs highlighted in the X-ray CT images (right side of Fig. 5) appeared drained (empty) in the corresponding MRI images (left side of Fig. 5). According to pore geometry and characteristics of the surrounding matrix, a vug can appear empty or with a "ring" of water, concentrated in the microporous matrix around the biggest pore.

At whole core scale, neither corrected porosity nor fracture density show a straightforward relationship with measured permeabilities supporting the belief that in these carbonates the porous space architecture affects permeability more than the total amount of effective porous volume and no single parameter can be considered "key" to fully explain the heterogeneity system.
Fig. 6-8 show examples for in situ-bioherm (MBDST), fine grained (GRST/PKST) and coarse grained (RDST) reworked bioherm.
- MBDST - samples with very poor poro/perm characteristics; the relatively few vugs are connected mainly through the microporous matrix, which represents the main controlling factor for permeability.
- GRST/PKST - fairly good samples with a strong anisotropy as for permeability. The KTmax direction (between 0°-30°) does not correspond to the direction in which enlarged and elongated pores seem to be aligned; the effect of the few but well-defined fractures cutting the sample is probably prevalent.
- RDST – sample with a strong anisotropy: permeability measured in the 0° direction is four orders of magnitude greater than permeability in the 90° direction. Similar disparity is noted between Kv and KTmax. The tomographic images highlight the dominant presence of touching vugs derived from the enlargement of growth framework pores within clasts and interparticle pores between clasts.

The analysis of the complete data set suggests the following general rules:
- in MBDST the permeability is mainly controlled by the matrix, in bioherm-related GRST/PKST by microfracturing and in RDST by touching vugs .
- MBDST samples show the narrowest range of permeability values, in contrast to the wide scattering registered in the other samples (mainly RDST) ; this can be read as an index of anisotropy and/or directionality.
- strong anisotropy in K values is mainly related to fracturing and/or touching vugs.

As already shown, the highlighted textural differences among MBDST, GRST/PKST and RDST correspond to a significantly different order of magnitude of permeability: about one, tens and hundreds of millidarcies, respectively, as reported in Tab. 2.

The effect of confining stress was not investigated; we expect different behaviour for the three lithotypes. We can hypothesize a greater effect on the tightest samples, in particular in the presence of fractures (MBDST and RDST facies).

CONCLUSIONS

Dealing with such complex porous networks, whose "objects" often have dimension exceeding the sample (thin section, plugs but also whole core) dimension, it is known that single measurements are not fully representative and classical statistical approaches can often lead to misleading conclusions/interpretations.

This study confirms the need to approach these samples in an unconventional way, utilizing different, appropriate tools at different scales of observation and combining the data/observations to acquire a confident template of the poro/permeable system and decide the average characteristics more representative of each defined litho type.

Also tomographic tools alone cannot solve the problem, but they have to be considered an important part of the process of effective characterization. As for the specific studied samples we found that:

- reworked biohermal-related facies do not necessarily have higher porosities than in-situ bioherms, but they probably have more efficient fluid flow pathways
- there is only a fair relationship between P21 (relevant to open features) and KTmax; fractured samples may reach permeability values up to tens of millidarcies; however, microfracturing cannot be considered the main controlling factor of permeability
- even if, at the core scale, in situ (MBDST) and reworked (RDST) facies can have very similar poro/perm values, they are the result of different porous space architectures: the dynamic properties at larger scale is still an open question, which requires further investigation
- in this phase of the work we did not take into account other important information, such as textural aspects from image logs and dynamic data from wellbore (mud losses, WFT, PLT). Their integration with core data is a further step to pursue
- these considerations are consistent with the investigated data set; we are aware that, to extend them to the field scale, a larger data set and integration with well bore data are necessary.
- dissolution porosity calculation results are not representative due to the problem of water loss from core during the MRI acquisition.
- Future development of this methodology will also include quantitative measurement of vuggy porosity and assessment of fluid flow patterns through improved image processing of 3D tomographic data.
- For future acquisition with MRI, we have to use a special rubber core holder with caps to avoid the water loss from central vugs during the long time acquisition.

ACKNOWLEDGEMENTS

REFERENCES

1. Bona N., Radaelli F., Ortenzi A., De Poli A., Peduzzi C., Giorgioni M. : "Estimating Petrophysical Properties in a Complex Fractured Reservoir " – *Journal of Petroleum Technology*, June 2002, pag. 44
2. Bona N., Radaelli F., Ortenzi A., Giorgioni M.: "Integrated Core Analysis for Fractured Reservoirs: Quantification of Storage and Flow Capacity of Matrix, Vugs, and Fractures" SPE Reservoir Evaluation & Engineering, August 2003, pag. 226 (SPE 85636)
3. Bye A., L., Rennan L.S, Widerøe H. C., Boassen T., Ringen J. K. "Residual Gas Distribution In Vuggy Carbonate by Use of X-Ray CT, NMR and Cryo-ESEM" SCA 2008-46 presented at SCA Symposium in Abu Dabi, UAE, 2008
4. Forbes P. "Centrifuge Data Analysis Techniques : a SCA Survey on the Calculation of Drainage Capillary Pressure Curves from Centrifuge Measurements" SCA 1997-14 presented at SCA Symposium in Calgary, Canada, 1997
5. Hidajat I., Mohanty K. K., Flaum M., Hirasaki G. J. "Study of Vuggy Carbonates Using NMR and X-Ray CT Scanning" SPE Reservoir Engineering, Oct. 2004, pag. 365
6. Hirasaki G. J., O'Meara D.J., Rohan J.A. "Centrifuge Measurements of Capillary Pressure: Part 1 - Outflow Boundary Condition" SPE Reservoir Engineering, Feb. 1992, pag. 133
7. Jennings J. "Petrophysical Variability, Fluid-Flow Behaviour, and the Implications for Analysis and Modeling of Carbonate Reservoirs" & "A Geologist's Introduction to Permeability Averaging and the Effects of Scale on the Permeability of Heterogeneous Rocks" 2008-09 AAPG Distinguished Lecture.
8. Knackstedt M., Arns C., Ghous A., Skllariou A., Senden T., Sheppard A., Sok R., Averdunk H., Val Pinczewski W., Padhy G., Ioannidis M. "3D Imaging and flow characterization of the pore space of carbonate core samples" SCA2006-23 presented at SCA Symposium in Trondheim, Norway, 2006
9. Mattiello D., Balzarini M., Ferraccioli L., Brancolini A. "Calculation of constituent porosity in a dual-porosity matrix: MRI and image analysis integration" SCA 1997-06 presented at SCA Symposium in Calgary, Canada, 1997
10. Martinez-Angeles R., Hernandez-Escobedo L., Perez-Rosales C. "3 D Quantification of Vugs and Fractures Network in Limestone Cores" SPE 77780 presented at the SPE Annual Technical Conference and Exhibition held in San Antonio, Texas, 2002
11. Radaelli F., Balzarini M., Nicula S., and Ortenzi A. "Rock Structure Characterisation Through Imaging Techniques Integration" SPE 50569, presented at the 1998 SPE European Petroleum Conference held in The Hague, The Netherlands, 20-22 October 1998
12. Vik B., Djurhuus, Spildo K, Skauge A. "Characterisation of Vuggy Carbonates" SPE 111434 presented at the SPE/EAGE Reservoir Characterization Conference held in Abu Dabi, UAE, 23-31 Oct. 2007
13. Withjack E. M., Devier C, Michael G. "The Role of X-Ray Computed Tomography in Core Analysis" presented at the SPE Western Regional/AAPG Pacific Section, Long Beach, California, U.S.A., 19–24 May 2003.

14. Vizika O., Youssef S., Rosenberg E. , Gland N., Bekri S. "Multiscale Approach for Shaping an Efficient EOR/IOR Field Management, from Lab to Reservoir" IFP-OAPEC Joint Seminar *Improved Oil Recovery Techniques and Their Role In Boosting The Recovery Factor* Rueil-Malmaison, France, 26-28 June 2007

Lithocode	Transversal permeability (angle)						Kv	Porosity, %	
	0	30	60	90	120	150			
M-BDST	< 0.01	0.93	1.39	0.17	0.76	0.23	1.84	5.13	V
M-BDST	6.30	0.41	0.03	0.72	2.27	33.82	54.59	6.77	G,V
M-BDST	1.77	1.78	1.69	2.03	2.00	2.14	2.07	6.89	G,V
M-BDST	3.23	1.80	1.89	2.27	1.88	1.10	< 0.01	4.87	G,V,F
GRST/PKST	0.76	1.52	1.61	1.19	1.16	1.99	0.85	0.86	G,V
GRST/PKST	0.65	1.46	2.50	1.15	0.57	6.35	9.91	2.61	I,V
GRST/PKST	0.56	0.86	0.66	0.59	0.67	0.74	1.07	5.97	I,V
GRST/PKST	20.24	32.70	2.80	4.77	2.80	0.02	4.03	8.58	I,V
GRST/PKST	1.02	3.03	4.91	6.49	1.87	2.60	1.78	8.87	I,V
RDST	< 0.01	1.55	0.05	0.05	0.89	< 0.01	0.12	10.3	G,V,I
RDST	18.67	21.04	22.49	16.12	16.63	29.38	223.87	4.78	V,G
RDST	1.54	1.34	1.98	1.64	1.99	1.51	< 0.01	6.79	G,V
RDST	4.36	1.15	0.25	0.83	0.08	1.84	0.11	6.83	G,V,F
RDST	934.13	735.40	596.78	0.56	0.12	652.51	0.88	3.66	G,V,F
RDST	1040.31	615.20	6.99	142.50	858.41	900.27	0.701	5.06	G,V

Legend: G: growth porosity
F: fracture porosity
I: interparticle porosity
V: vuggy porosity

Table 1– Petrophysical data of the samples

Sedimentological description	Litho code	Type of porosity (visual estimate)	Average porosity %	Perm. range (md) (in whatever direction)
In-situ biohermal deposits	MBDST	Growth Vuggy	5.9	<0.01-55
Reworked biohermal, fine grained deposits	GRST/PKST	Interparticle Vuggy	5.4	0.02-33
Reworked biohermal, coarse grained deposits	RDST	Growth Vuggy Fracture related	6.2	<0.01-1040

Table 2 – Mean data values for the depositional facies
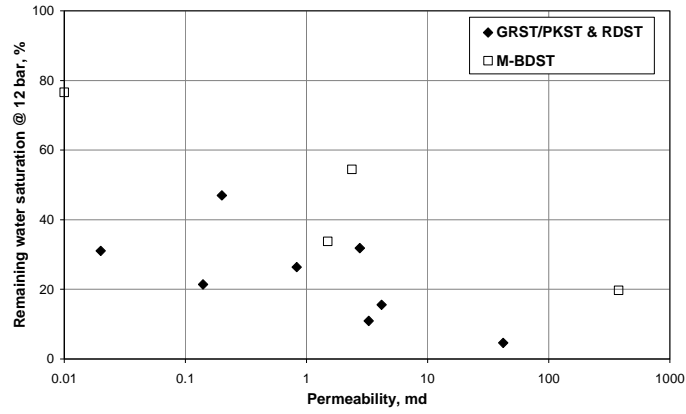
Fig. 1 – Remaining water saturation after drainage @ 12 bar
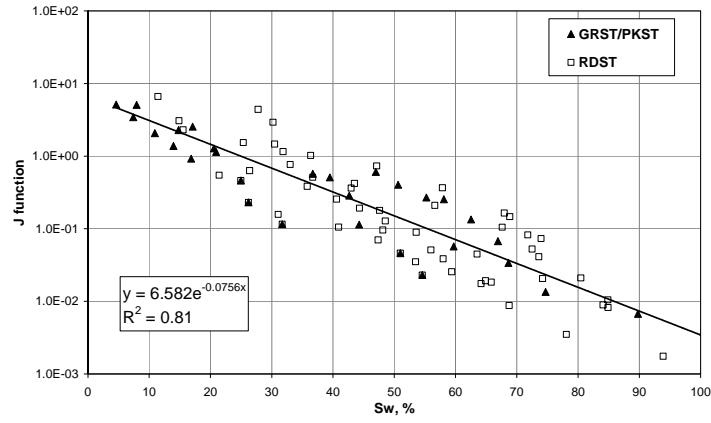
Fig. 2 – J function for GRST/PKST and RDST facies
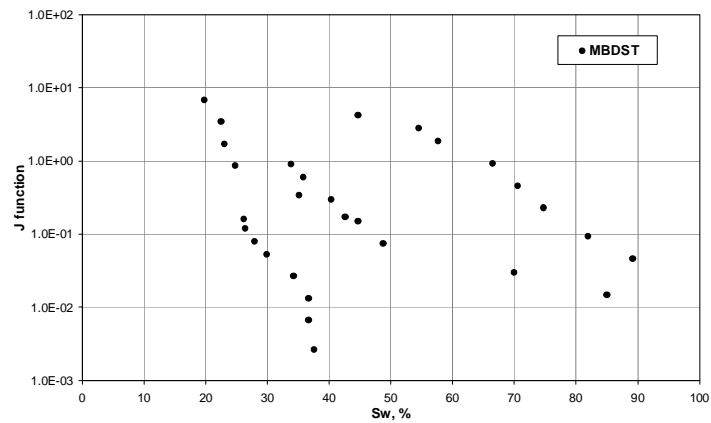
Fig. 3– J function for MBDST facies

360° unrolled picture of the external core surface

360° unrolled X-Ray image obtained very close to the external core surface
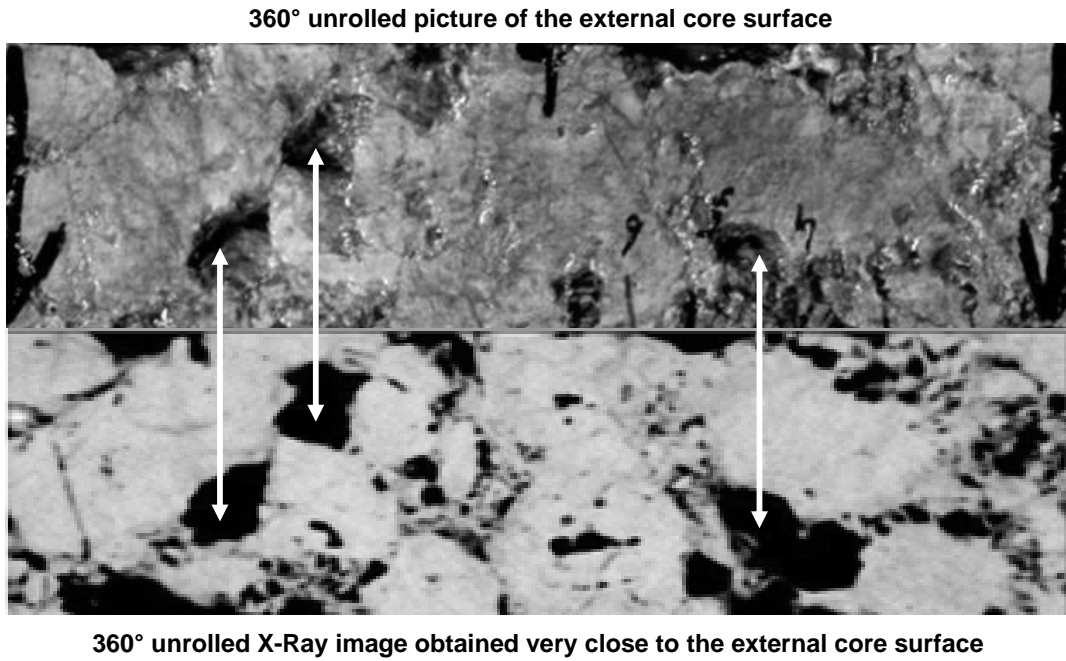
Fig. 4 Comparison between 360° unrolled picture of the external surface (upper) and corresponding unrolled X-ray CT image (lower) showing the presence of large vugs

A1   B1

A2   B2
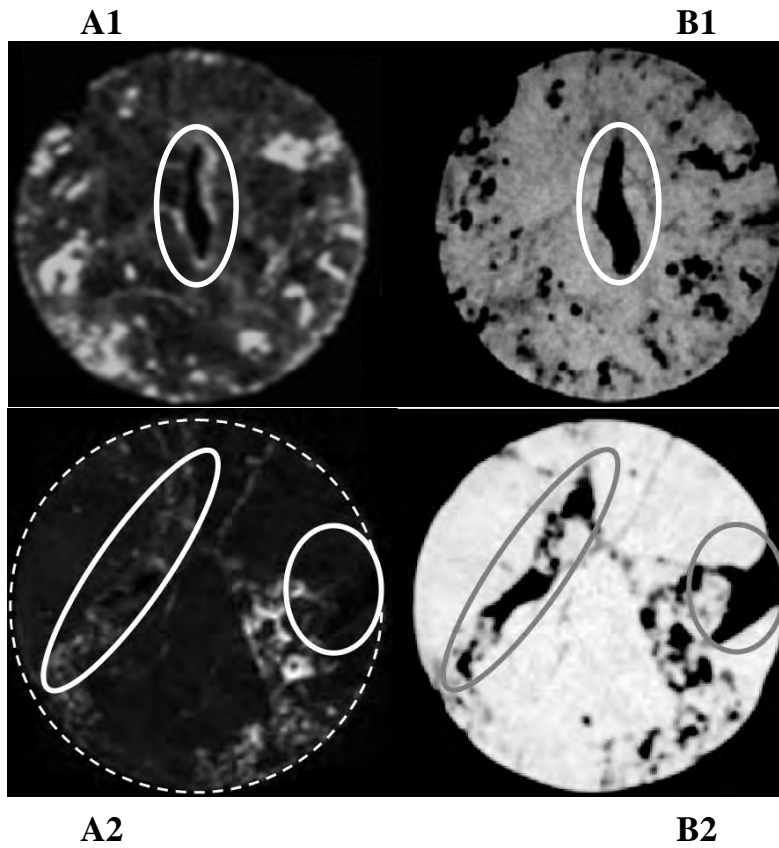
Fig. 5 – Comparison between MRI (A1–A2) and X-ray CT (B1–B2) images taken in the same sample slice
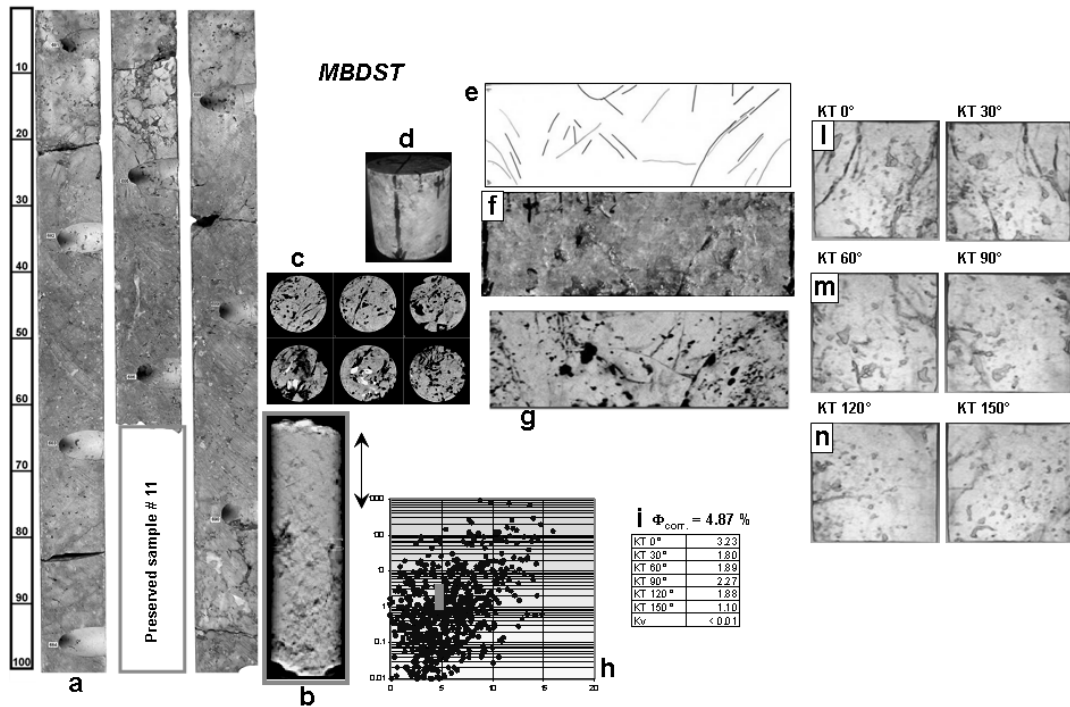
Legend:

a = slabbed core photo;

b = -X ray CT pilot image of preserved core interval;

c = X-ray CT transversal slices;

d = whole core selected sample;

e = fracture traces observed on the external core surface;

f = unrolled 360° external core surface photo;

g = corresponding unrolled 360° X-ray CT image;

h = porosity vs. permeability cross plot;

i = transversal permeability values;

l, m, n = 2D X-ray CT images corresponding to the direction of KT measurements;

o = direction of "good" permeability

Fig. 6 - Example for in situ-bioherm (MBDST)
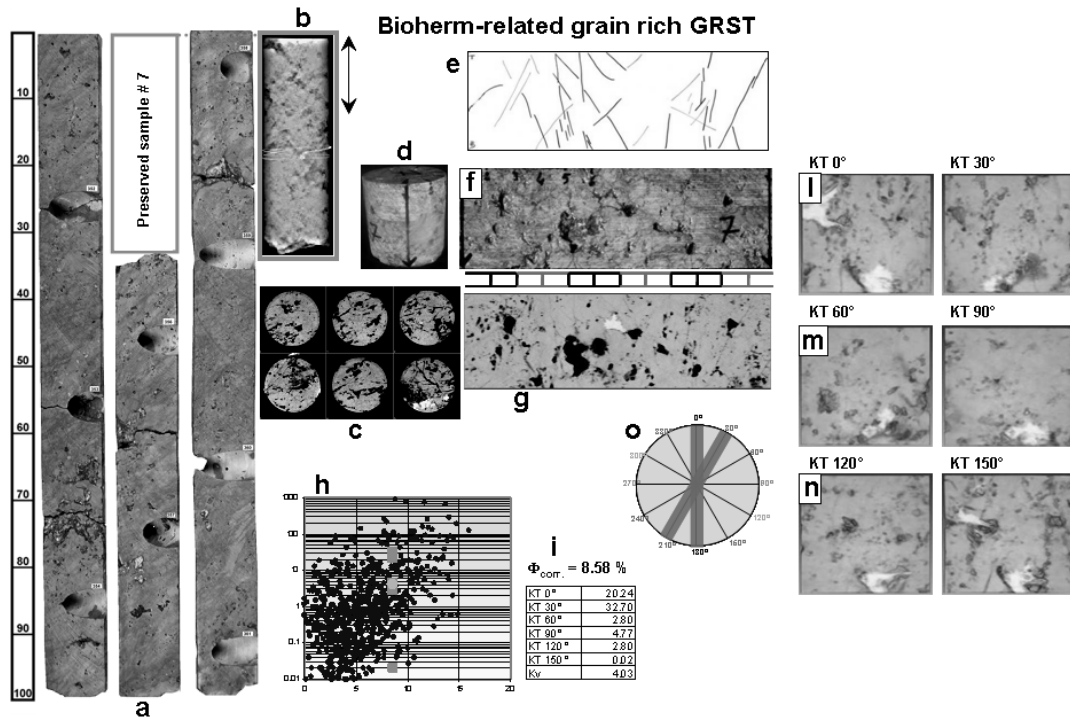
Fig. 7 - Example for fine grained (GRST/PKST) reworked bioherm (Legend as Fig. 6)
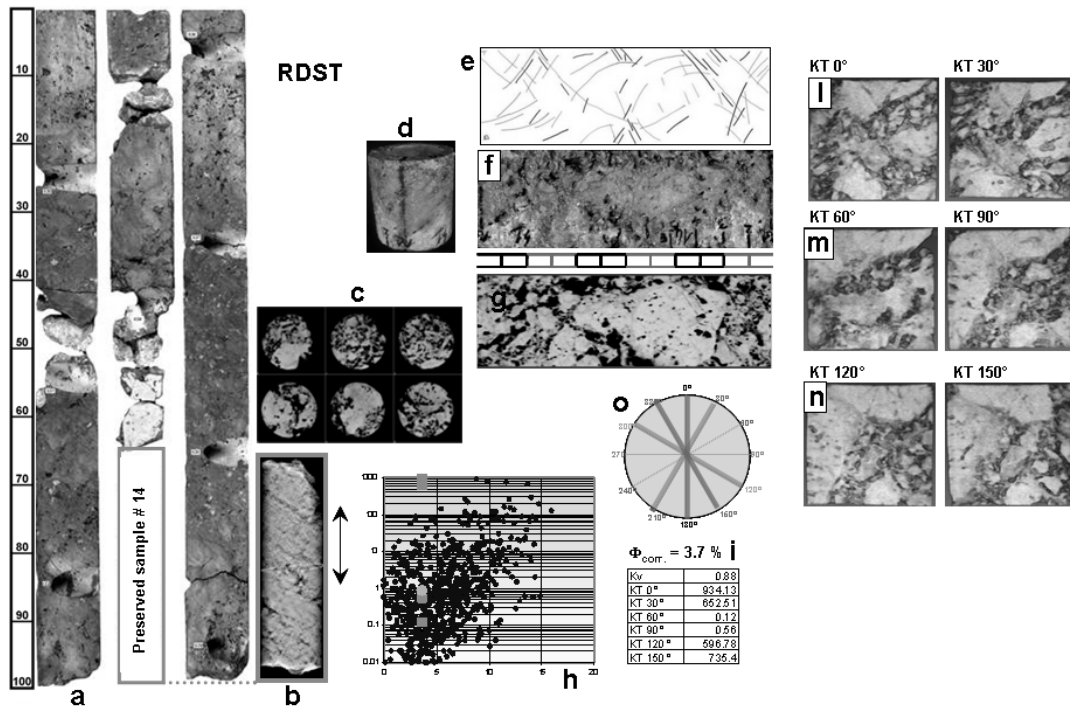
Fig. 8 - Example coarse grained (RDST) reworked bioherm (Legend as Fig. 6)